Cell Reports, Volume *43*

Supplemental information

The ULK1 effector BAG2 regulates autophagy initiation by modulating AMBRA1 localization

Devanarayanan Siva Sankar, Stephanie Kaeser-Pebernard, Christine Vionnet, Sebastian Favre, Lais de Oliveira Marchioro, Benjamin Pillet, Jianwen Zhou, Michael Stumpe, Werner Josef Kovacs, Dieter Kressler, Manuela Antonioli, Gian Maria Fimia, and Jörn Dengjel

The ULK1 effector BAG2 regulates autophagy initiation by modulating AMBRA1 localization

Devanarayanan Siva Sankar[1], Stephanie Kaeser-Pebernard[1], Christine Vionnet[1], Sebastian Favre[1], Lais Oliveira De Marchioro[3,4], Benjamin Pillet[1], Jianwen Zhou[2], Michael Stumpe[1], Werner Josef Kovacs[2], Dieter Kressler[1], Manuela Antonioli[3, 5], Gian Maria Fimia[3, 6], Jörn Dengjel[1]*

[1] Department of Biology, University of Fribourg, 1700 Fribourg, Switzerland

[2] Institute for Molecular Health Sciences, ETH Zurich, 8093 Zürich, Switzerland

[3] Department of Epidemiology, Preclinical Research and Advanced Diagnostics, National Institute for Infectious Diseases IRCCS "L. Spallanzani", 00149 Rome, Italy

[4] Department of Pharmacology, Federal University of São Paulo (UNIFESP), São Paulo, Brazil, CEP 05508-000

[5] Department of Biology, University of Rome "Tor Vergata", 00133 Rome, Italy

[6] Department of Molecular Medicine, University of Rome "Sapienza", 00185 Rome, Italy

*Lead contact and corresponding author: Jörn Dengjel, joern.dengjel@unifr.ch

Supplemental Figures:

Supplemental References

Suppl Figure S1

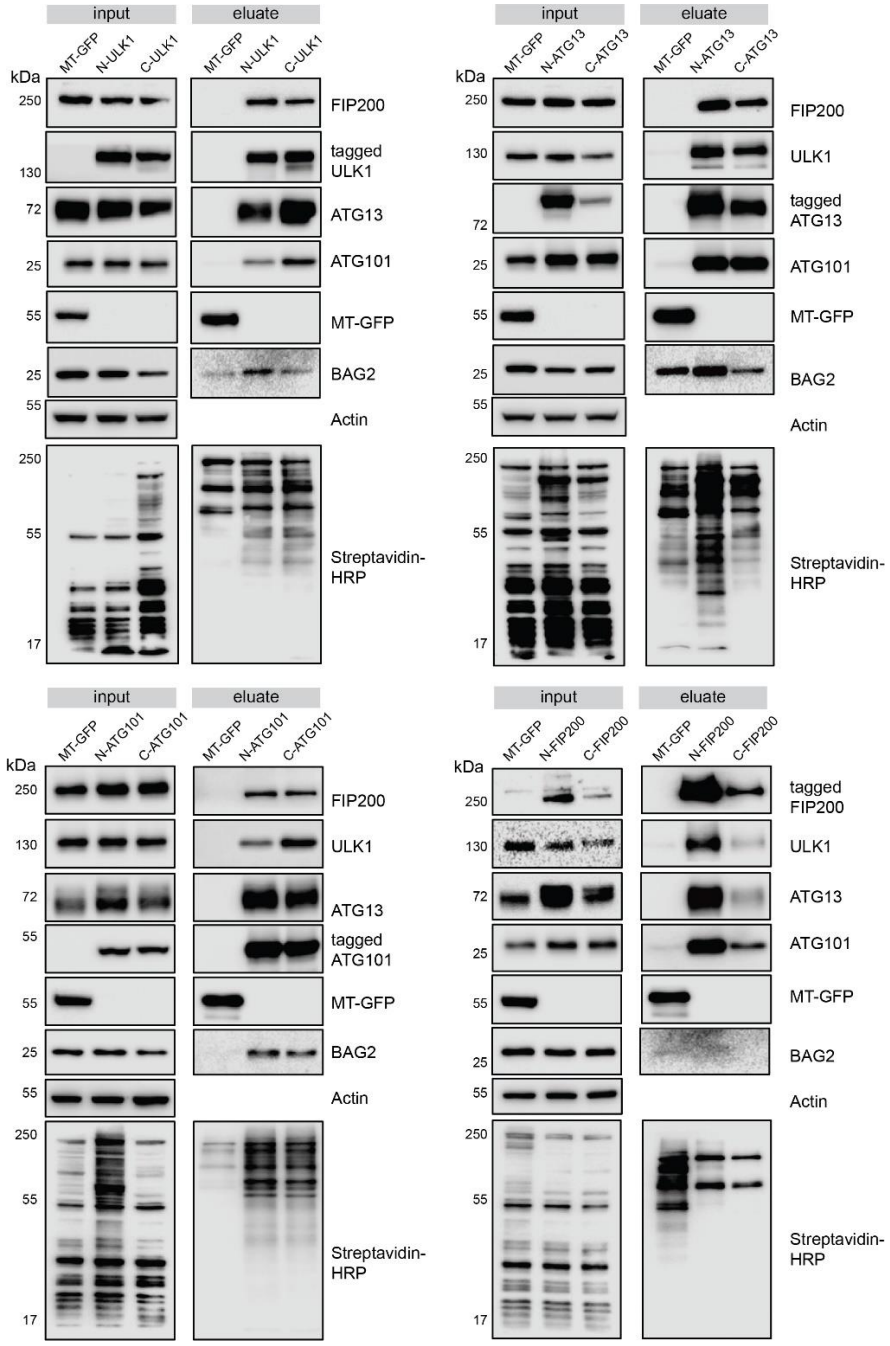

Supplemental Figure S1: Streptavidin enrichment of miniTurbo-based biotinylation reactions of ULK1 complex members. CRISPR KO HeLa cells of ULK1 complex members were used to express indicated N-/C-terminal miniTurbo fusion constructs. Streptavidin-based APs were performed followed by western blot analysis. Input and eluates are shown in respective figures and Streptavidin-HRP was used to detect biotinylation reactions. MT-GFP was used as negative control in respective CRISPR KO cell lines along with the indicated bait proteins.

Suppl Figure S2

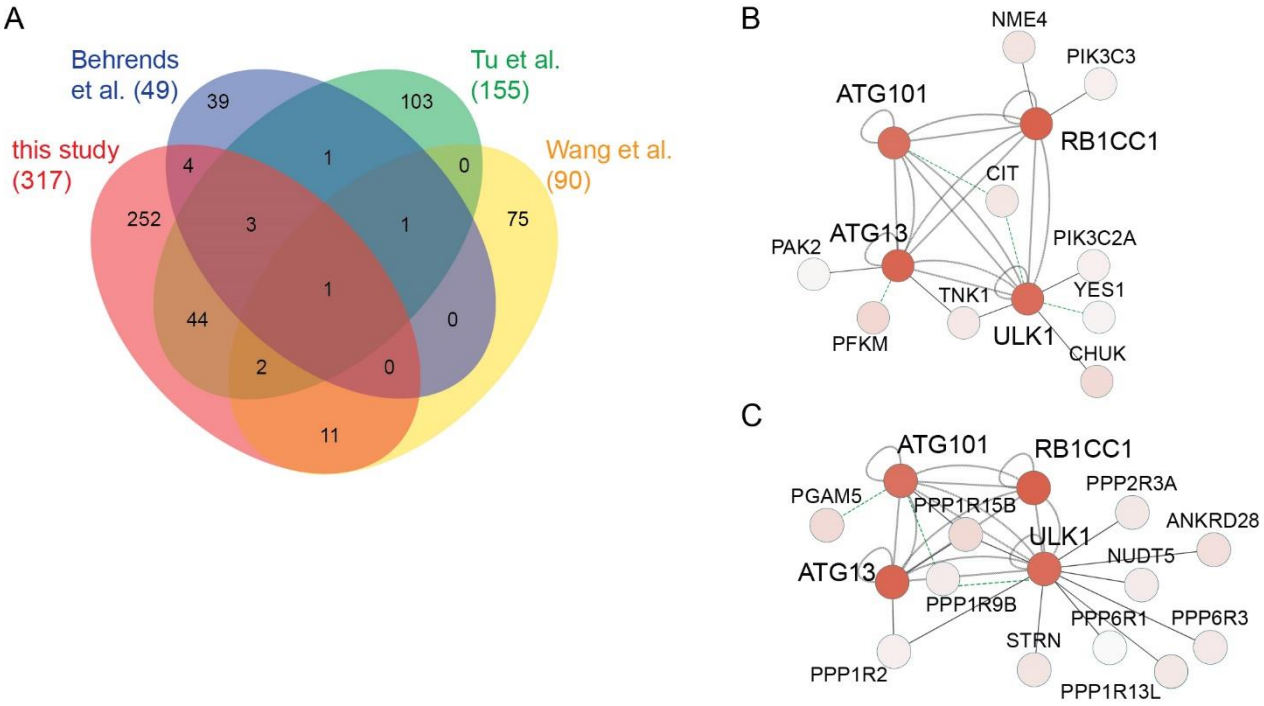

Supplemental Figure S2: Deep ULK1 complex interactome. (A) Comparison of the current ULK1 complex deep interactome with existing studies. The overlap of the current studies with published data is larger than the overlap between respective data sets [S1-3]. Numbers in brackets indicate total numbers of hits of respective studies. **(B)** Protein- and lipid-kinases identified as ULK1 complex interactors in the current study (see Figure 2). Whereas the PI3P generating kinase PIK3C3/VPS34 is a well-known target of ULK1 [S4], it is not known if ULK1 also phosphorylates PIK3C2A, another PI3P generating kinase which has been shown to induce autophagy in response to shear stress [S5]. The alpha subunit of the inhibitor of NFκB kinase CHUK/IKKA has been shown to be degraded by autophagy [S6] and to promote AMBRA1-ATG8 interaction in mitophagy [S7]; however, a direct crosstalk with ULK1 has not been described. This is also true for the tyrosine protein kinase YES1, which was shown to promote autophagy in ovarian cancer [S8], and for the protein kinases CIT, PAK2 and TNK1, which have been linked amongst others to cytoskeleton regulation but not to autophagy. **(C)** Phosphatase subunits identified as ULK1 complex interactors in the current study (see Figure 2). Four of these, PPP1R2, PPP6R3, PPP1R13L and STRN were identified by us as ULK1 targets, the PP2a regulatory subunit STRN being involved in positive feedback promoting the dephosphorylation and activation of ULK1 [S9].

Suppl Figure S3

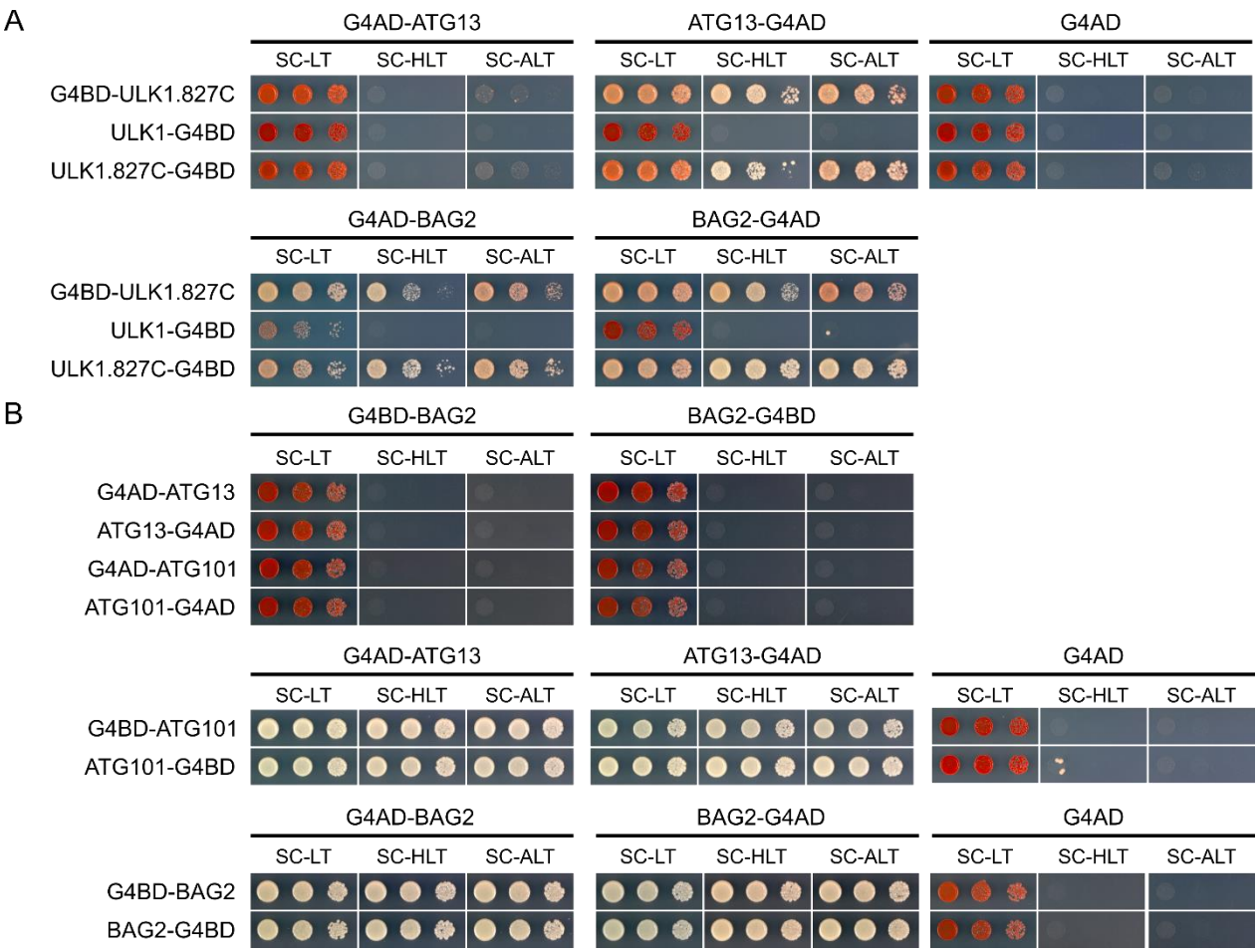

Supplemental Figure S3: Assessment of protein-protein interactions by yeast two-hybrid (Y2H) assays. The Y2H reporter strain PJ69-4A was transformed with two plasmids expressing the human proteins of interest fused to the Gal4 activation domain (G4AD) or Gal4 DNA-binding domain (G4BD) at either their N- or C-terminal end. Transformed cells were spotted in 10-fold dilutions series onto SC-Leu-Trp (SC-LT), SC-His-Leu-Trp (SC-HLT), SC-Ade-Leu-Trp (SC-ALT) plates, which were incubated for 3 d at 30°C. **(A)** ATG13 (positive control) and BAG2 interact with the C-terminal domain of ULK1 (abbreviated as ULK1.827C); however, no interaction is observed with full-length ULK1. **(B)** BAG2 neither directly interacts with ATG13 nor ATG101, while the known ATG13-ATG101 and BAG2-BAG2 interactions could be recapitulated by the Y2H assays. Note that none of the tested fusion proteins exhibit self-activation of the reporter genes, as indicated by the absence of growth when these are co-expressed with the non-fused G4AD or G4BD.

Suppl Figure S4

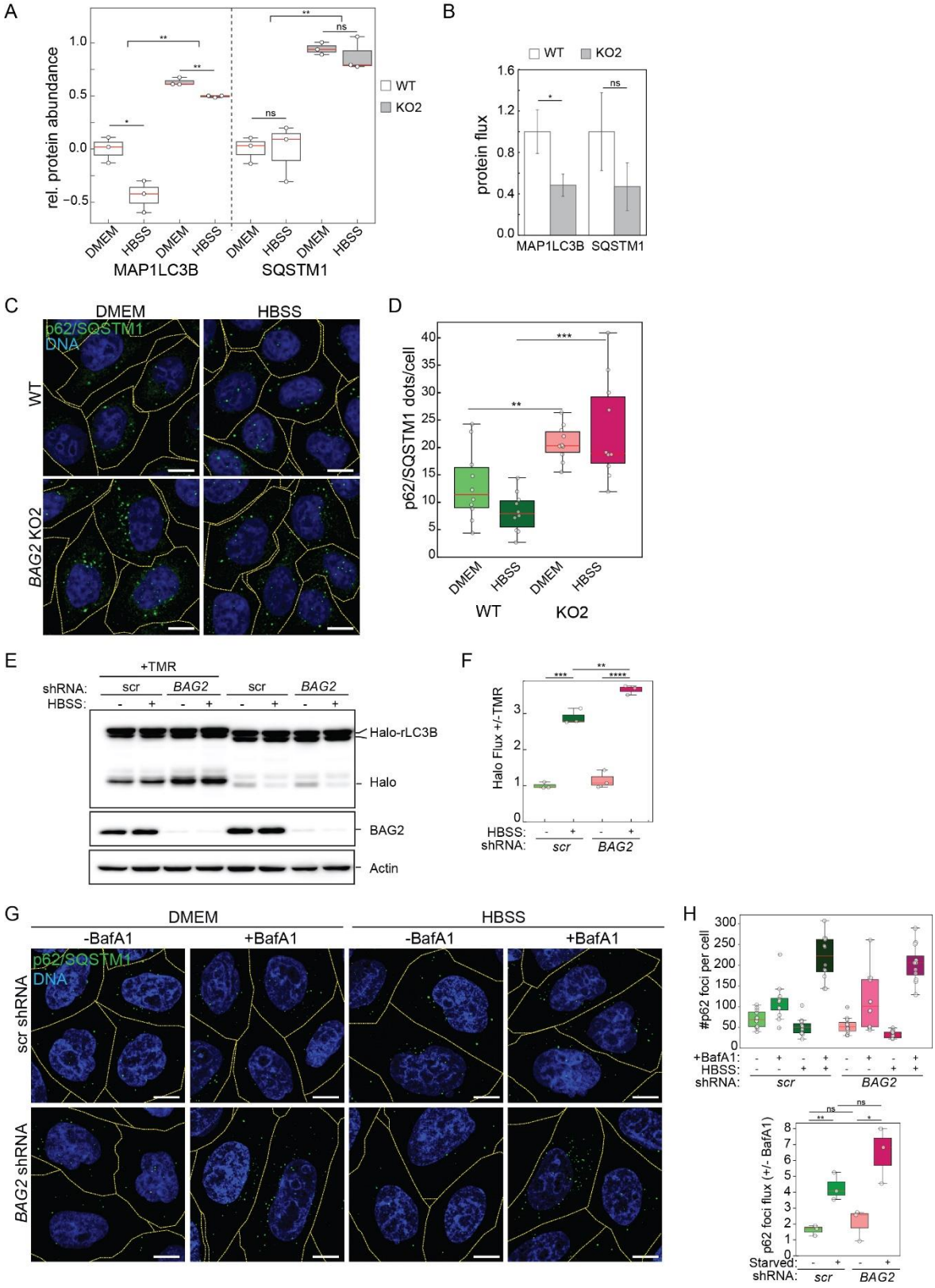

Supplemental Figure S4: Perturbed autophagy flux upon loss of BAG2. (A) Differential abundance of autophagy relevant proteins in *BAG2* KO cells. Chronic loss of BAG2 leads to an increase of MAP1LC3 and SQSTM1 protein levels. Quantitative MS data of n=3 biological replicates. **(B)** KO of BAG2 reduces protein turnover. Quantitative MS data of n=3 biological replicates. Cells were starved for 2 h with or without the presence of 10 nM ConA. Protein fluxes represent the abundance ratios of ConA compared to non-ConA samples. Error bars indicate SD. *: p<0.05, LIMMA. **(C-D)** SQSTM1/p62 dot formation analyzed by IF. Fluorescent micrographs showing p62/SQSTM1 foci formation in *BAG2* WT and KO HeLa cells in untreated (DMEM) or starved (HBSS, 3h) conditions (C). Scale bar= 10 μm. One representative image out of n=3 biological replicates is shown. (D) Quantification of p62/SQSTM1 foci count per cell as shown in (C). White dots represent the average foci count per cell and per biological replicate (n=3). A minimum of 20 cells were counted per slide, and a minimum of 3 slides were imaged per replicate. A two-way ANOVA test followed by a TukeyHSD post-hoc test was used to identify significant differences. **: p ≤ 0.01, ***: p ≤ 0.001. **(E)** Halo-LC3 assay using WT HeLa cells transgenic for an inducible Halo-LC3 construct, transduced with either *scrambled*- or *BAG2* shRNA-expressing lentiviruses, then pulsed for 30 min with 100 nM TMR and either incubated in full growth medium (DMEM) or starvation medium (HBSS) for 3 h. One representative assay out of n=3 biological replicates is shown. An increase in molecular weight is observed for the Halo-LC3 and Halo fragments when TMR ligand is conjugated. **(F)** Quantification of the Halo autophagic flux in (E), corresponding to the ratio of Halo tag released in presence vs in absence of TMR (+/-). White dots: individual biological replicates, n=3. An unpaired two-tailed Student's t-test was used to compare values. **: $p \leq 0.01$; ***: $p \leq 0.001$; ****: $p \leq 0.0001$. **(G)** Fluorescent micrographs showing p62/SQSTM1 foci formation in WT HeLa cells transduced with either *scrambled*- or *BAG2* shRNA-expressing lentiviruses, in untreated (DMEM) or starved (HBSS, 3h) conditions supplemented or not with 2nM BafA1. Scale bar= 10 μm. One representative image out of n=3 biological replicates is shown. **(H)** Quantification of p62/SQSTM1 foci count per cell as shown in (G). White dots represent the average foci count per cell and per image. 4 images were quantified per biological replicate (n=3), totaling a minimum of 30 cells per condition and per replicate. A two-way ANOVA test followed by a TukeyHSD post-hoc test was used to identify significant differences. *: p ≤ 0.05, **: p ≤ 0.01, ns: not significant.

Suppl Figure S5

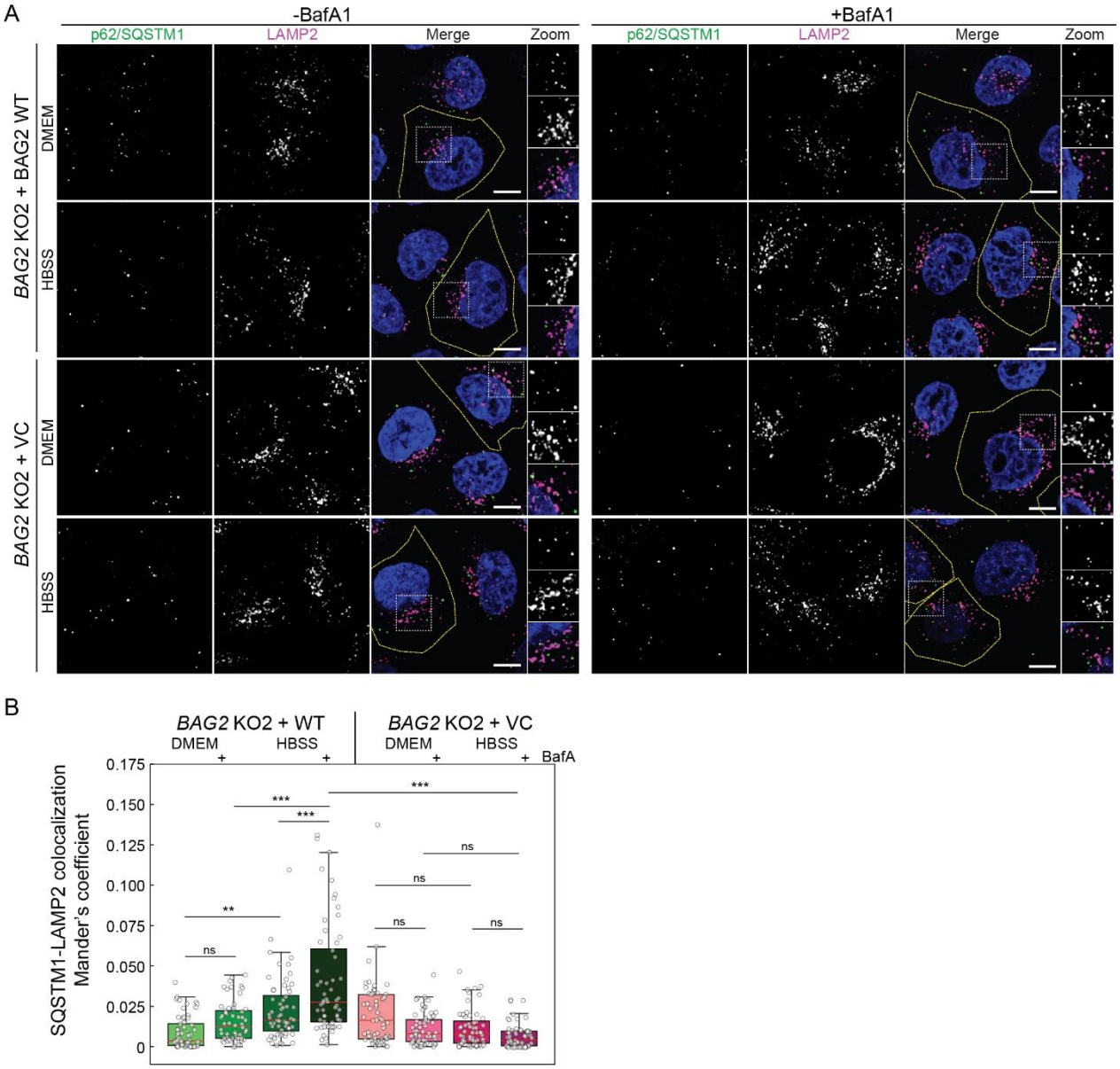

Supplemental Figure S5: Perturbed autophagosomal-lysosomal targeting upon chronic loss of BAG2. (A) SQSTM1/p62 colocalization with lysosomal marker LAMP2 analyzed by IF. Fluorescent micrographs showing p62/SQSTM1 colocalization with LAMP2 in BAG2 KO HeLa cells stably transduced with inducible BAG2 WT or an empty vector control (VC), in untreated (DMEM) or starved (HBSS, 3 h) conditions, supplemented (+) or not with Bafilomycin A1 (BafA1, 2 nM, 3 h). Scale bar= 10 μm. One representative image out of n=3 biological replicates is shown. **(B)** Quantification of p62/SQSTM1 colocalization with LAMP2 per cell as shown in (A). White dots represent the thresholded Mander's coefficient per cell, corresponding to the fraction of LAMP2 signal colocalizing with p62/SQSTM1 signal. A total of 20 cells per

condition and biological replicate were measured (n=3). A two-way ANOVA test followed by a TukeyHSD post-hoc test was used to identify significant differences. **: $p \leq 0.01$, ***: $p \leq 0.001$, ns: not significant.

Suppl Figure S6

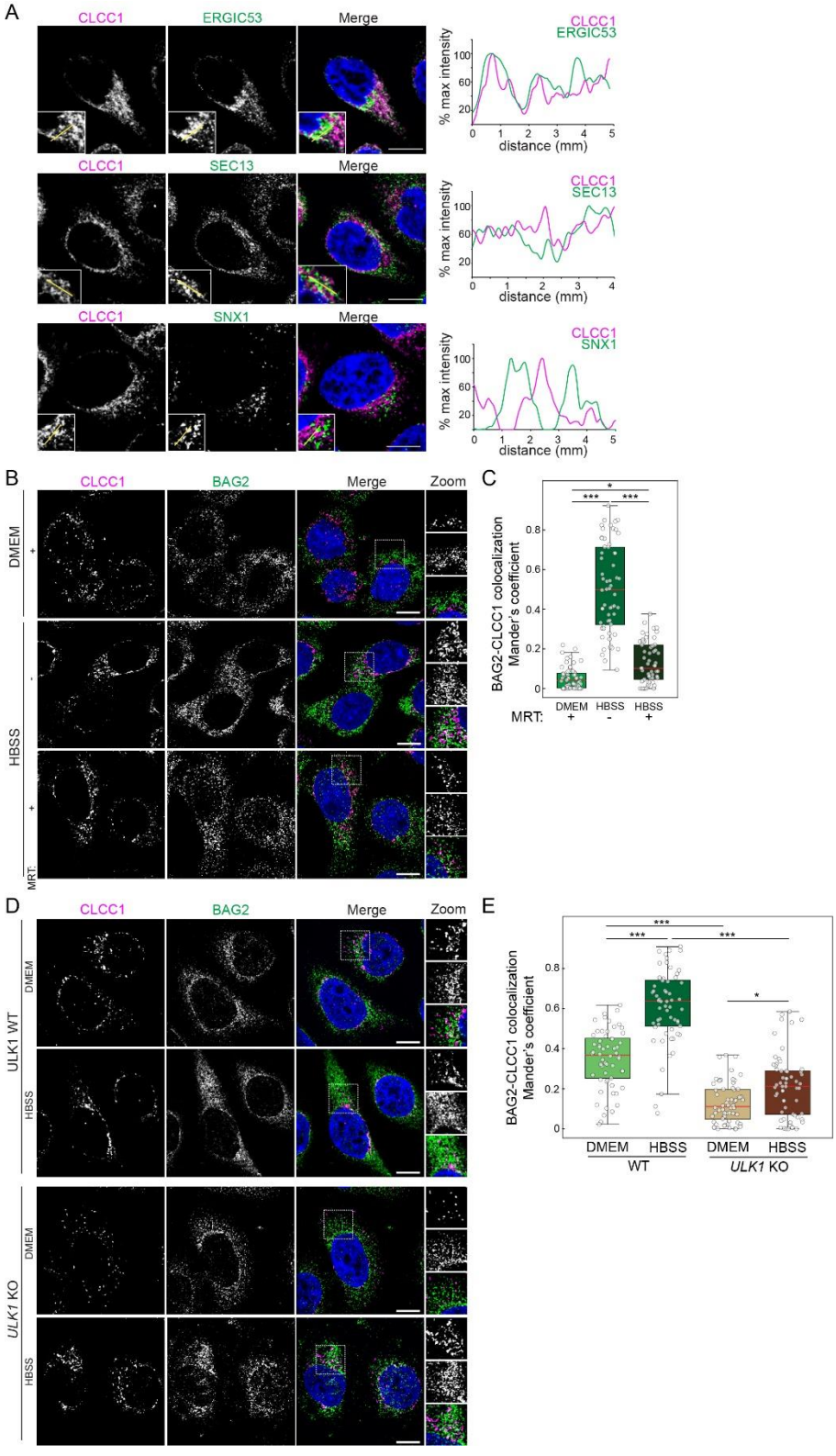

Supplemental Figure S6: Colocalization of CLCC1 with organellar markers and BAG2. (A) Colocalization of CLCC1 with organellar markers. CLCC1 partially colocalizes with ERGIC53 and SEC13, but not with SNX1. Left panels: fluorescent micrographs from HeLa WT cells in fed conditions, labeled using the indicated primary antibodies. Yellow lines: line drawings used to generate plot profiles. Right panels: plot profiles corresponding to the yellow lines. The signal of each fluorophore was normalized to their maximum intensity to obtain comparable profiles between antibodies. Scale bar= 10 μm. **(B-E)** Colocalization of CLCC1 with BAG2 is ULK1 activity dependent. (B-C) BAG2 colocalization with ER marker CLCC1 analyzed by IF. Fluorescent micrographs showing BAG2 colocalization with CLCC1 in WT HeLa cells treated 2 h in DMEM + ULK inhibitor MRT68921 (2 h, 20 μM), then incubated for 2 more hours either in DMEM + ULK inhibitor (DMEM +), or starved in HBSS without (HBSS -) or with inhibitor (HBSS +). Scale bar=10 μm. One representative image out of n=3 biological replicates is shown. (C) Quantification of BAG2 colocalization with CLCC1 per cell as shown in (B). White dots represent the thresholded Mander's coefficient per cell, corresponding to the fraction of CLCC1 signal colocalizing with the BAG2 signal. A total of 20 cells per condition and biological replicate were measured (n=3). A two-way ANOVA test followed by a TukeyHSD post-hoc test was used to identify significant differences. (D-E) BAG2 colocalization with ER marker CLCC1 analyzed by IF. Fluorescent micrographs showing BAG2 colocalization with CLCC1 in HeLa WT or ULK1 KO cells in untreated (DMEM) or starved (HBSS, 3 h) conditions. Scale bar= 10 μm. One representative image out of n=3 biological replicates is shown. (E) Quantification BAG2 colocalization with CLCC1 per cell as shown in (D). White dots represent the thresholded Mander's coefficient per cell, corresponding to the fraction of CLCC1 signal colocalizing with the BAG2 signal. A total of 20 cells per condition and biological replicate were measured (n=3). A two-way ANOVA test followed by a TukeyHSD post-hoc test was used to identify significant differences. *: $p \leq 0.05$, ***: $p \leq 0.001$, ns: not significant.

Suppl Figure S7

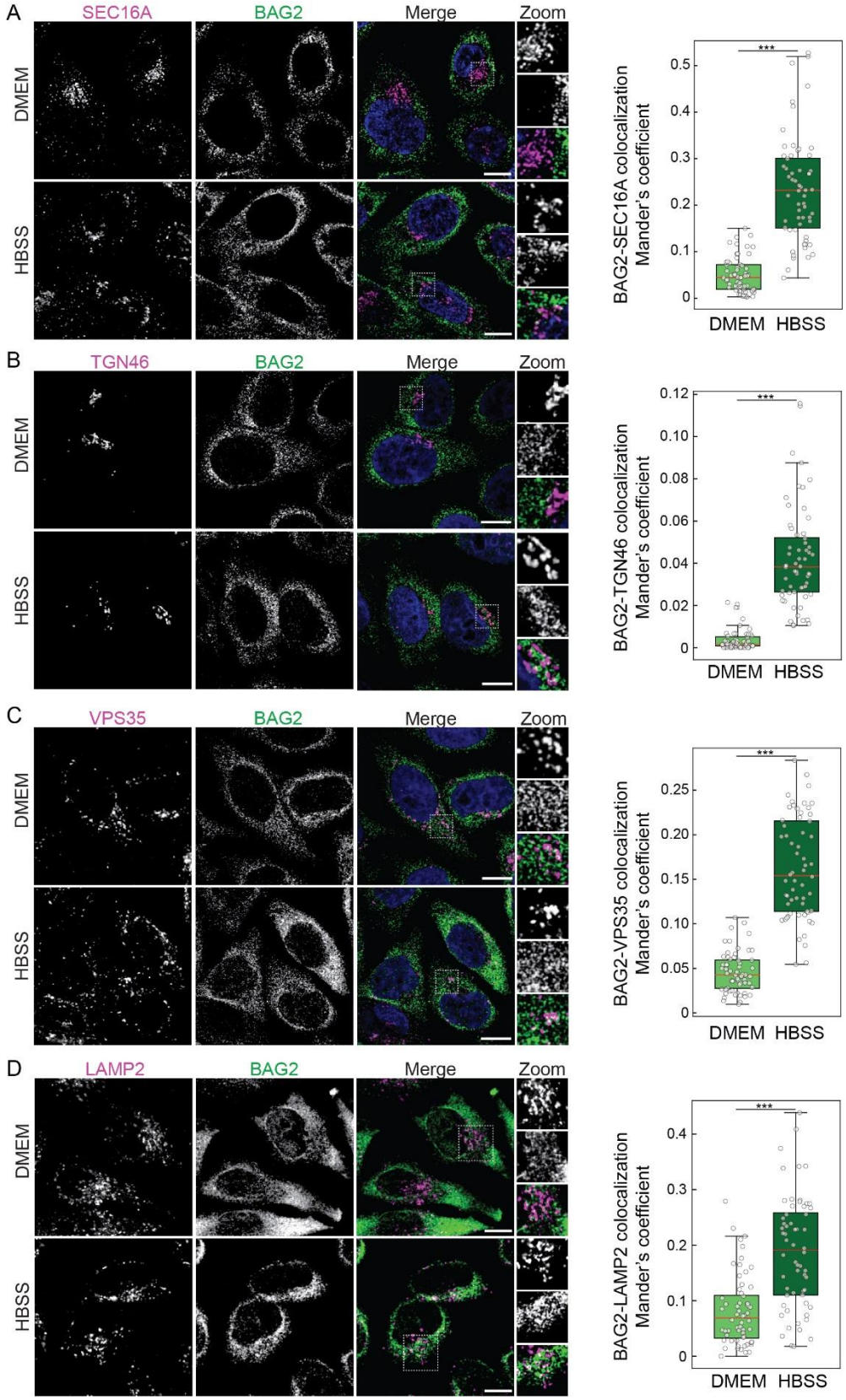

Supplemental Figure S7: Increased localization of BAG2 to endomembranes in starvation conditions. (A-D) Fluorescent micrographs labeled with indicated primary antibodies. In starved cells (HBSS, 2 h) the BAG2 colocalization with endomembrane markers increases compared to fed cells (DMEM), indicating increased localization to endomembranes. A total of 60 cells per condition were measured in n=3 biological replicates and are represented by white dots, reflecting the thresholded Mander's coefficient per cell, corresponding to the fraction of indicated protein signal colocalizing with the BAG2 signal. Representative pictures are shown. Scale bar= 10 μm. A two-way ANOVA test followed by a TukeyHSD post-hoc test was used to identify significant differences. ***: $p \leq 0.001$.

Suppl Figure S8

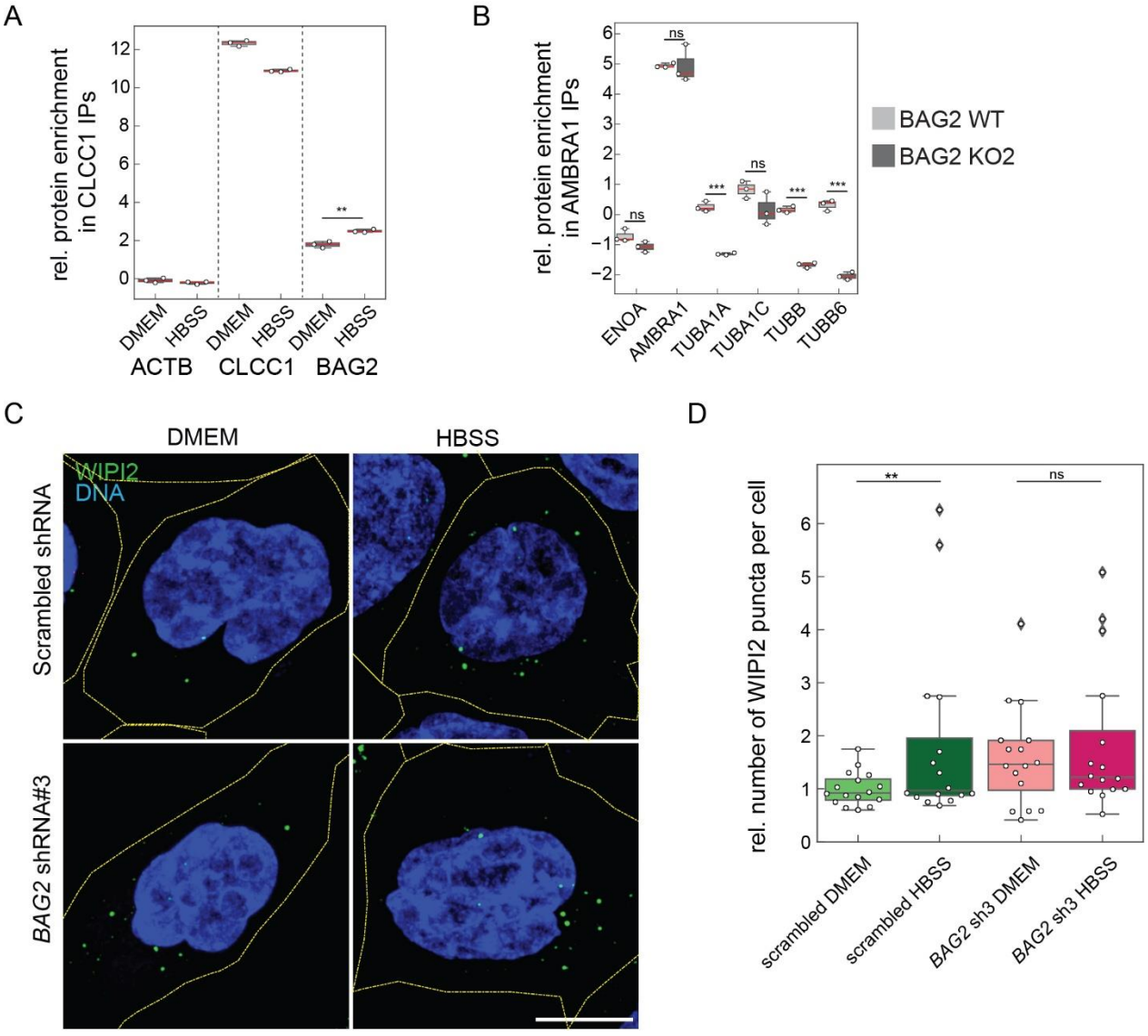

Supplemental Figure S8: Effects of BAG2 loss on protein interactions and WIPI2 localization. (A) Protein levels in endogenous CLCC1 IPs. BAG2 binds stronger to CLCC1 under starvation conditions (2 h of HBSS treatment). AMBRA1 was not identified in CLCC1 IPs. Quantitative MS data of n=3 biological replicates. Protein abundances are normalized to median abundances of respective experiment. Shown is enrichment relative to IgG control experiments, ACTB is shown as negative control. **(B)** Protein levels in endogenous AMBRA1 IPs. Loss of BAG2 leads to reduced binding of AMBRA1 to indicated tubulins. Quantitative MS data of n=3 biological replicates. ENOA is shown as negative control. IPs were normalized to AMBRA1 levels. Unpaired student's t-test were used to determine significant differences. ns: not significant, **: p<0.01, ***: p<0.001. **(C-D)** Acute loss of BAG2 leads to increased number of WIPI2 dots. (A) WIPI2 puncta analysis

using IF micrographs from untreated (DMEM) or starved (HBSS, 3 h) HeLa WT treated with a scrambled control shRNA and an anti-BAG2 shRNA. Representative pictures of n=4 biological replicates are shown. Scale bar= 10 μm. (B) Puncta quantification of (A). Each white dot represents the quantified average WIPI2 dots per cell per image (8 to 19 cells per image), with a total of 16 images (4 images per condition), per replicate of n=4 biological replicates. Scale bar = 10 μm. A two-way ANOVA test followed by a TukeyHSD post-hoc test was used to identify significant differences. **: $p \leq 0.01$, ns: not significant.

Supplemental References

S1. Behrends, C., Sowa, M.E., Gygi, S.P., and Harper, J.W. (2010). Network organization of the human autophagy system. Nature *466*, 68-76. 10.1038/nature09204.

S2. Tu, Y.X.I., Sydor, A.M., Coyaud, E., Laurent, E.M.N., Dyer, D., Mellouk, N., St-Germain, J., Vernon, R.M., Forman-Kay, J.D., Li, T., et al. (2021). Global Proximity Interactome of the Human Macroautophagy Pathway. Autophagy, 1-13. 10.1080/15548627.2021.1965711.

S3. Wang, B., Maxwell, B.A., Joo, J.H., Gwon, Y., Messing, J., Mishra, A., Shaw, T.I., Ward, A.L., Quan, H., Sakurada, S.M., et al. (2019). ULK1 and ULK2 Regulate Stress Granule Disassembly Through Phosphorylation and Activation of VCP/p97. Mol Cell *74*, 742-757 e748. 10.1016/j.molcel.2019.03.027.

S4. Egan, D.F., Chun, M.G., Vamos, M., Zou, H., Rong, J., Miller, C.J., Lou, H.J., Raveendra-Panickar, D., Yang, C.C., Sheffler, D.J., et al. (2015). Small Molecule Inhibition of the Autophagy Kinase ULK1 and Identification of ULK1 Substrates. Mol Cell *59*, 285-297. 10.1016/j.molcel.2015.05.031.

S5. Boukhalfa, A., Nascimbeni, A.C., Ramel, D., Dupont, N., Hirsch, E., Gayral, S., Laffargue, M., Codogno, P., and Morel, E. (2020). PI3KC2alpha-dependent and VPS34-independent generation of PI3P controls primary cilium-mediated autophagy in response to shear stress. Nat Commun *11*, 294. 10.1038/s41467-019-14086-1.

S6. Tan, Q., Zou, S., Jin, R., Hu, Y., Xu, H., Wang, H., Ding, M., Hu, M., Wei, C., and Song, L. (2020). Selective degradation of IKKalpha by autophagy is essential for arsenite-induced cancer cell apoptosis. Cell Death Dis *11*, 222. 10.1038/s41419-020-2420-5.

S7. Di Rita, A., Peschiaroli, A., P, D.A., Strobbe, D., Hu, Z., Gruber, J., Nygaard, M., Lambrughi, M., Melino, G., Papaleo, E., et al. (2018). HUWE1 E3 ligase promotes PINK1/PARKIN-independent mitophagy by regulating AMBRA1 activation via IKKalpha. Nat Commun *9*, 3755. 10.1038/s41467-018-05722-3.

S8. Zhou, Y., Wang, C., Ding, J., Chen, Y., Sun, Y., and Cheng, Z. (2022). miR-133a targets YES1 to reduce cisplatin resistance in ovarian cancer by regulating cell autophagy. Cancer Cell Int *22*, 15. 10.1186/s12935-021-02412-x.

S9. Hu, Z., Sankar, D.S., Vu, B., Leytens, A., Vionnet, C., Wu, W., Stumpe, M., Martinez-Martinez, E., Stork, B., and Dengjel, J. (2021). ULK1 phosphorylation of striatin activates protein phosphatase 2A and autophagy. Cell Rep *36*, 109762. 10.1016/j.celrep.2021.109762.